



Final Draft
of the original manuscript:

Vaidya, W.V.; Horstmann, M.; Venzke, V.; Petrovski, B.; Kocak, M.;
Kocik, R.; Tempus, G.:

**Improving interfacial properties of a laser beam welded dissimilar
joint of aluminium AA6056 and titanium Ti6Al4V for
aeronautical applications**

In: Journal of Materials Science (2010) Springer

DOI: 10.1007/s10853-010-4719-6

Improving interfacial properties of a laser beam welded dissimilar joint of aluminium AA6056 and titanium Ti6Al4V for aeronautical applications

W. V. Vaidya^{*1}, M. Horstmann¹, V. Ventzke¹, B. Petrovski¹, M. Koçak¹, R. Kocik², G. Tempus²

¹GKSS Research Centre Geesthacht,
Institute of Materials Research,
Materials Mechanics,
Max-Planck-Strasse 1,
D-21502 Geesthacht,
Germany

²AIRBUS Operations GmbH,
Metal Technology,
Airbus-Allee 1,
D-28199 Bremen,
Germany

*Corresponding author
E-mail: waman.vaidya@gkss.de
Tel.: 0049 4152 872600,
Fax.: 0049 4152 872534

Authors' e-mail addresses:
waman.vaidya@gkss.de, manfred.horstmann@gkss.de, volker.ventzke@gkss.de,
blagoj.petrovski@gkss.de, mkocak@gedik.com.tr, rainer.kocik@astrium.eads.net and
dr.tempus@airbus.com

Abstract

Dissimilar welds of aluminium alloy AA6056 and titanium alloy Ti6Al4V were produced by a novel technique. AA6056 sheet was machined at one end to a U-slot shape, enabling the intake of the Ti6Al4V sheet. The Al-alloy U-slot was then butt welded by split laser beam without using a filling wire, thus making a weld by melting only the Al-alloy. Thereby the intermetallic brittle phase $TiAl_3$ formed at the weld interface and affected mechanical properties. As a continuation of the previous work, the joint design was modified by chamfering Ti6Al4V to reduce the formation of interfacial $TiAl_3$. It is shown in this work how this seemingly insignificant joint modification has refined microstructure and increased hardness and strength. The most impressive feature was the improved resistance to fatigue crack propagation whereby the fracture type in the fusion zone of AA6056 adjacent to the weld interface changed from partially intercrystalline to completely transcrystalline. Possible metallurgical processes leading to the property improvements are discussed.

Keywords:

Dissimilar weld; Fatigue crack propagation; Mechanical properties; Microstructure; Weld interface

1 Introduction

Dissimilar joints can provide application-oriented solutions. The combination of an Al-alloy with Ti6Al4V for aircraft seat tracks, shown in Fig. 1, is such an application while reducing weight (Al-alloy) and improving strength and corrosion resistance (Ti6Al4V). Previously we have reported our approach of laser beam welding for this target application [1,2], and structure-property relationships of welded laboratory coupons [3,4]. In continuation, here we show how the joint properties of the weld interface, which are generally dominated by intermetallic phases formed in the reaction zone [5], can be improved through a modified design.

Welding of dissimilar metals successfully is already a challenge due to differences in physical, chemical and metallurgical properties of the base materials used, and finding the optimum process parameter window continues to be the basic prerequisite (e.g. [6-8]). When a non-ferrous material such as aluminium is involved, *brittle* intermetallic phases form very often at the weld interface [5]. This is a very common phenomenon in dissimilar welds with aluminium as one of the base materials, not only in fusion welding [9,10] and irrespective of energy input either global as in arc welding [9] or local as in resistance spot welding [10], but, also in solid state welding, e.g. in friction [11] and friction stir welds [12,13]. Inherently, weld interfaces are already associated with sharp changeovers in properties [5]. Due to phases formed, the reaction zone [14] or its vicinity [15] or both may become susceptible for cracks under tensile loading as found in fusion welds of aluminium–steel [14] and aluminium–titanium [15]. When phases formed are also brittle, interfacial performance may be degraded in combination with weld defects. Typical consequences in dissimilar welds can be reduced fatigue life [16,17], increased fatigue crack propagation [18,19] and decreased fracture toughness [19].

Aluminium-titanium joints can be produced by different techniques [1-4,15,20-32]. Techniques such as brazing [20], friction welding [21,22], diffusion bonding [23,24] or explosive welding [25] are due to form and size restrictions unsuitable for the seat track, (see Fig. 1), which, when realized, is going to be a long length linear weld (up to a few meters). Friction stir welding of Ti6Al4V with an Al-alloy could be attractive, but, has just surpassed the feasibility study stage [26] and is far from applications. Hence, the most feasible near future application is fusion welding. However, according to the literature [27,28], the fusion weldability of aluminium to other metallic materials does not appear to be so straightforward. For example, whereas *pure* Al and Ti could be fusion welded by electron beam, these welding parameters could not be transferred for welding the respective *alloy* combinations [29]. In

laser beam welded aluminium-titanium joints defects such as cracks or porosity [30,31] and non-uniform seam morphology [15,32] have been reported. Fortunately, through process modifications, cracks can be avoided [30] and uniform seam thickness can be achieved [1-4].

The essential features of the welding technique developed at AIRBUS are shown schematically in Figs. 2a,b [1-3]. The Al-alloy sheet is machined at one end to a U-slot shape. This serves as the intake for the Ti6Al4V sheet. Subsequently, the laser split-beam, operated in the heat conduction mode, melts *only* the Al-alloy U-slot and the butt-weld is produced *without* a filler wire. The ability of this technique was demonstrated also by fabricating a one-meter long real seat track as in Fig. 1 (see Fig. 1c in [3]). The butt-weld configuration in a coupon is shown in Fig. 2c (referred to as “unmodified joint” hereafter) [3]. In contrast to the Al-side, the Ti-side remained practically unchanged, except for the Al/Ti-interface, on which a thin $TiAl_3$ layer of about $1.8 \mu m$ was formed. The tensile fracture was confined to the hardness dip in the heat-affected zone on the Al-side. A pullout or an interfacial fracture such as that reported recently for fusion welded joints of ferritic steel and an Al-alloy [33], fabricated by the cold metal transfer (CMT) technique [34], was not observed. Thus, the weld interface was strong and mechanically stable [3,4] and the laser beam welding technique used [1,2] appropriate.

The formation of intermetallic phase(s) [5], as in other combinations with aluminium [9-14], is also common in aluminium-titanium joints [1-4,15,20-24,26-30,32]. When a brittle phase such as $TiAl_3$ is formed at the weld interface, deformation becomes difficult, which may lead to uncontrolled debonding in the presence of an interfacial crack. This was not observed in fracture mechanics tests [4]. Insofar the joint quality of the weld interface against cracking was found to be good. Its *ranking* was, however, the lowest when compared for fatigue crack propagation and fracture toughness in the changeover between the fusion zone and the heat-affected zone [4]. The immediate remedy *without* changing the welding

parameters was to reduce the vertical interfacial area as shown in Fig. 2d (referred to as “modified joint” hereafter). The extent of the brittle phase being reduced, an improved performance was anticipated. On the other hand, it was unclear, whether a slanted surface (45° chamfer) would affect wetting and become prone to weld defects such as pores. This may favour debonding and instead of improvement, properties would have then been degraded.

As a continuation of the previous work [3-4] the configuration in Fig. 2d is investigated and compared with that in Fig. 2c for microstructure, hardness variations, tensile strength and performance in terms of fatigue crack propagation and fracture toughness. In the following, the term “interface” refers to the welded vertical Al/Ti-seam (see the “notch location” in Figs. 2c,d shown by the vertical line). The terminology “welding” [35] has been retained here, since at least one of the base materials was melted (and since filler wire was not used, it is not considered exactly as “brazing”, “braze welding” [36], or “welding-brazing” [15,32]). Relevant information has been provided again, so as to avoid cross-referring. Although questions about statistical validation are open, this study shows how the joint properties can principally be improved, at least on the laboratory scale.

2 Experimental procedure

The experimental procedure was kept unchanged [3-4] so as to facilitate the comparison. The base material compositions are shown in Table 1. AA6056 is a new fusion weldable aerospace alloy that can be precipitation hardened to different strength levels [37,38]. Ti6Al4V is already a widely used alloy in aerospace. From thicker sheets, material for welding was machined. AA6056 was peak-aged (T6: $190\text{ }^\circ\text{C}\text{-}4\text{h/air}$; hardening by $\beta''/\beta'+Q'$) and had uniform thickness of 2 mm with machined U-slot at one end as shown in Fig. 3a. The latter was used as the intake for Ti6Al4V. Ti6Al4V was mill annealed and had a thickness of 1.8 mm. The joint gap for the sheet insertion was less than 0.4 mm. The sheets

had length 330 mm and width 47 mm, and were cleaned, degreased and pickled before welding as per the aeronautic standards.

Sheets were welded to coupons as shown in Figs. 2a,b using a split beam 4 kW Nd:YAG laser in the heat conduction mode at BIAS in Bremen, Germany, with parameters shown in Table 2. The advantage of beam splitting is the feasibility of welding from both sides with *one* laser, for which otherwise *two* lasers would have been required. The beam axis was perpendicular to the U-slot and the beam was positioned mainly on the Al-side such that the lower end of the beam was about 1 mm below the inserted edge of the Ti6Al4V sheet. Thereby only the U-slot on the Al-side was melted and filler wire was not used. The maximum temperature measured with thermocouples on the Ti-side was 995 °C in the unmodified joint and was slightly above the $\alpha+\beta \leftrightarrow \beta$ transus temperature. The welding process was very fast; on the Al-side, temperature dropped to 220 °C after about 27 s.

The coupons had the dimensions, length 330 mm and width 94 mm, as shown in Fig. 3b. Constancy of hardness on the Al-side was reached after 7 weeks of post weld natural ageing (GP zone formation; hardness increasing from about 65 VHN to about 92 VHN). This was reproducible, which in turn indicates consistency of the welding process and the microstructural development. Therefore, all coupons were first naturally aged for this time interval before testing. Specimens were extracted by electric discharge machining from a region that exhibited constancy in the welding process and the temperature field as inferred by microhardness (HV0.2) and by process simulation using finite element analysis. Due to the limited availability of the welded material, specimens were tested only in the as-welded condition without machining the excess weld material (Figs. 2c,d).

Microstructure was investigated by light optical microscopy and scanning electron microscopy (SEM) using energy dispersive X-rays (EDX) for local chemical analysis.

Metallographic specimens were etched concurrently and under the same conditions using Kroll's reagent for 20 seconds. Tensile tests were carried out on full-width strips $20 \times 94 \text{ mm}^2$ using a laser extensometer and simultaneously a commercial image analysis system [39] to capture the instantaneous deformation pattern. For a given variant 3 specimens were tested.

To verify the joint quality against cracking, the notch was kept parallel to the weld and was positioned at the interface (shown by the vertical line in Figs. 2c,d; see Fig. 3b also). For fatigue crack propagation [40] and fracture toughness [41] testing, compact tension, C(T), specimens were used. Here, to reduce data variability, side grooving can be useful to restrict crack deflection. However, as mentioned above, such specimens were not tested due to the limited availability of the welded material. The specimens had initial notch length, $a_n = 10 \text{ mm}$, width, $W = 50 \text{ mm}$ and as-welded full thickness ($= B$). As shown in Fig. 3b, fatigue crack propagation specimens had a straight notch; those for fracture toughness testing had similar dimensions, but the notch was longer (22.5 mm) and modified in the load line for a gauge insertion and the distance between the loading holes was longer [42]. At least two specimens for a given variant were tested to improve data reliability. For comparison, base material specimens were tested and had the same overall dimensions as those for the welded ones.

After cutting and machining to dimensions, initial bending present in a coupon became less in specimens. So as to avoid the effect of bending and near zero or below zero loading, a high load ratio value, $R (= P_{\min}/P_{\max})$, was used for fatigue crack propagation testing and P_{\min} value controlled closely. The average R value was 0.4 ± 0.05 . Specimens were tested using servo-hydraulic machines at a frequency $f = 10 \text{ Hz}$ and under ambient laboratory conditions at room temperature. The standard ASTM E647 [40] was followed for specimen dimensions and testing. The starting ΔK value at the notch was 10 MPavm for all specimens ($B_{\text{Al-side}} = 2 \text{ mm}$). The data up to a crack length $a = 24 \text{ mm}$ were considered for evaluation, although data were

acquired over a longer crack length. Crack length was measured indirectly and continuously by using an on-top extensometer for maximum crack opening displacement (COD_{max}) and calibrated against the optical crack length [4]. The polynomial was then used for crack length calculation. Such polynomial was obtained for each specimen.

For fracture toughness testing the initial notch length, $a_n = 22.5$ mm, was extended by fatigue pre-cracking ($\Delta a \geq 2.5$ mm) to introduce a sharp crack and to reach the value $0.5W$ (= 25 mm). Specimens were tested using servo-hydraulic and electro-mechanical machines in the laboratory air and at room temperature using the GKSS procedure [42]. This procedure is similar to ASTM E561 [41], but is modified additionally by a local crack tip opening displacement gauge (CTOD δ_5) technique [43]. The advantage is that the information is obtained *directly* on the crack tip and does not have to be inferred from the load line gauge, which is due to strength mismatch particularly important for dissimilar joints as in the present case. Hence, local CTOD values are used to describe fracture toughness. Extensive fractographic investigation was undertaken to understand the failure process particularly for fatigue crack propagation. Thereby the fracture half of the Ti-side was examined, since it was easier to identify adhering Al-particles and thus assess the bond characteristics.

3 Results and discussion

The welded coupons were free from surface defects such as spatter or undercut and the weld surface was clean and smooth. Internal defects such as cold shuts were not observed and in this sense the coupons were sound. Some isolated micro-pores (≤ 0.2 mm) or short chains of micro-pores were occasionally observed in the fusion zone. That such pores form is very common for the laser beam Al-welds due to entrapped gaseous impurities, particularly hydrogen [44]. Once a coupon was cut, the initial distortion was reduced significantly and the specimens were nearly straight.

3.1 Hardness gradient

The material condition of AA6056 before welding (T6: peak-aged) and the welding parameters (Table 2) were the same for both joint designs. This is reflected in the similarity of the hardness trend shown in Figs. 4a,b. Hardness on the Ti-side remained nearly constant (335 VHN). Since changes occurred on the Al-side, only these data are shown. Major changeovers in the hardness trend were as follows: the initial drop (fusion zone: up to about 3 mm from the interface), the increase followed by a drop (primary heat affected zone: up to about 7 mm from the interface), the steady increase (secondary heat affected zone: up to about 23 mm from the interface) followed by the constancy (base material in T6). Hardness of the modified joint was higher than that of the unmodified joint (Figs. 4a,b).

The possible correlation between hardness and hardening constituents is shown schematically in Fig. 4c. This presentation is based on the literature (for details see [3]). That initial precipitates coarsen or are dissolved and replaced by other constituents is very common, not only in welded precipitation hardenable Al-alloys (e.g. [45]), but also in welded superalloys such as Inconel 718 [46]. In AA6056, Mg, Si and Cu are the elements contributing to hardening phases Mg_2Si (β'' , β' , β) and $Al_5Cu_2Mg_8Si_6$ (Q' , Q) [37,38,47]. When peak-aged, the hardening is caused by metastable precipitates $\beta''/\beta'+Q'$. These are dissolved during laser beam welding (in the fusion zone and the heat affected zone), re-precipitate or transform during cooling as stable phases β and Q (in the fusion zone and the hardness dip), and coarsen and transform to $\beta'+Q'$ (in the secondary heat affected zone) due to heat flow. Thereafter, the initial precipitates are retained in the base material. The solute retained in the solid solution after welding forms GP zones on natural ageing and contributes to the increase in hardness. This process is more effective in the primary heat affected zone (which undergoes solution annealing during welding) than in the fusion zone, where the

solute is tied mostly as stable phases. That is why a defined natural ageing (for at least 7 weeks) was practiced to reach a stable material state.

To understand the solute distribution, the fusion zone was examined and was found to contain 3 types of large particles ($1 \mu\text{m} \leq d \leq 10 \mu\text{m}$); globular ($\leq 2 \mu\text{m}$) and lenticular ($\leq 5 \mu\text{m}$) within grains and lenticular ($\leq 10 \mu\text{m}$) at grain boundaries. Their analysis is shown in Table 3. All particles contained Cu, but had low Mg and Si in the grain boundary particles. The intragranular particles contained more Mg and Si, particularly the globular particles were enriched in Mg. Interestingly, although the solute was thus tied in these particles, there was still solute leftover in the particle-free matrix, which becomes available for GP zones on natural ageing as in the present case or for precipitates on post-weld ageing [3,48,49].

For a given position, particularly in the fusion zone and the primary heat affected zone, hardness in the modified joint specimen was higher on the Al-side up to about 10 VHN (data shown by triangles in Figs. 4a,b). With the same energy input (Table 2), the increase in volume of the Al-side coupled with reduced volume of the Ti-side (Figs. 2c,d) should have altered the thermal gradient and contributed to an increase in the rate of cooling. Due to reduced volume the temperature on the Ti-side during welding should have been higher, but aluminium, through its good thermal conductivity, should have steepened the thermal gradient, leading to a faster cooling. In turn, more solute is retained in the solution initially which coalesce subsequently to GP zones on post-weld natural ageing and contributes to increased hardness in the modified joint specimen (Figs. 4a,b). Hardness and strength may also increase depending on the grain size as per the Hall-Petch relationship (e.g. [50]). However, in the present case the change brought about by natural ageing should be the major contributor, since the hardness did increase on natural ageing (as mentioned in Experimental procedure) whereas the grain size at room temperature should not change over time.

3.2 Microstructure

As to be expected from the constancy of hardness, the Ti-side retained its initial microstructure (equiaxed α decorated with β) after welding. The Al-side, on the other hand, was significantly affected (Figs. 2,4). As regards property changes, the interfacial plane is the most critical location [5], particularly in the presence of a crack or a notch (Figs. 2c,d), since this is the site, where strain localization is going to occur due to different elastic moduli ($E_{Al} < E_{Ti}$). The Al-side, being weaker, was more prone to deformation than the Ti-side. Therefore, the fusion zone microstructure was investigated on the Al-side adjacent to the interface as shown in Fig. 5. The weld piece was mounted with the Al-side within the mount and the Ti-side was progressively removed by metallographic grinding and polishing until the Al-side just emerged. The area in Figs. 5c,d is estimated to be within 0.1 mm from the interface.

Except for the difference in grain size, the microstructure was otherwise comparable in both cases. While utilizing the orientation contrast in the back scattered electron mode, the average grain size, measured by the line intercept method, was found to be finer in the modified than in the unmodified joint (50 μm against 190 μm). Grain size in the fusion zone perpendicular to the interface in Figs. 2c,d was also smaller in the modified joint (40 μm) than in the unmodified joint (70 μm). These figures should be considered only as guideline values, since areas that could be investigated clearly in the unmodified joint were limited for an assertive statement. As discussed above, the thermal gradient due to changes in volume of titanium and aluminium seems to have induced a faster cooling rate in the modified joint and led to the difference in grain size in the fusion zone.

Additional possibility is the effect of solute Ti as the grain refiner during crystallisation [51-53]. Solute Ti, even in a small quantity (≥ 0.017 wt %) [52], is found to be a powerful inoculant for pure aluminium [51], and for laboratory and commercial Al-7Si foundry alloys

[52,53]. Just 10 °C before aluminium solidifies, TiAl_3 forms, nucleates aluminium grains and as aluminium solidifies, gets dissolved [51]. The Al-rich portion of the Al-Ti binary diagram shows that TiAl_3 forms by peritectic reaction of solid titanium with liquid aluminium [20,54]. While brazing, Si in molten aluminium restricts the dissolution of titanium, dissolves in TiAl_3 and reduces its growth [20]. From this it is tempting to speculate in the present case that if TiAl_3 formed is reduced in size by Si and transported into the fusion zone, it would act as a nucleating agent and reduce the grain size. Indeed, the faster cooling rate in the modified joint is likely to alter the fluid flow and the heat transfer characteristics of the weld pool, and assist this process.

The interfacial microstructure was very fine and could be studied only by SEM as shown in Fig. 6. As previously [3], the intermetallic phase in the reaction zone was identified as TiAl_3 by EDX analysis. Its width varied from 0.95 μm to 2.53 μm in the unmodified joint, and was slightly reduced ($0.85 \mu\text{m} \leq t \leq 1.81 \mu\text{m}$) in the modified joint specimen. We have analyzed a few areas and consider these values as a scatter, with the thickness of TiAl_3 at the interface in the modified joint as the lower bound. Non-uniform seam morphology as in welding-brazing [15,32] was, however, not observed. Insofar, the present welding method [1,2] is advantageous. Since TiAl_3 forms mainly while aluminium is in the liquid state [51,55], it follows that the faster the cooling rate, the shorter would be the interaction between the Al-melt and the Ti-side and the thinner would be TiAl_3 . Thus, Fig. 6b reconfirms that the cooling rate in the modified joint would have been faster. In both cases, β is still decorating α (as initially) on the Ti-side, which supports that the $\alpha+\beta \leftrightarrow \beta$ transformation did not occur during welding; otherwise, the morphology would have been different (say, interlaced plate or needle shaped Widmanstätten $\alpha+\beta$ structure due to fast cooling).

3.3 Strength and fracture toughness

Since hardness was somewhat higher and the microstructure slightly refined (Figs. 4,5), an improvement in strength was expected in the modified joint. For tensile testing the gauge length was divided into various sections as shown in the inset in Fig. 7a. It turned up that the Ti-side and to some extent the mixed zone exhibited only elastic behaviour, and all deformation occurred on the Al-side, including that in the fusion zone. Therefore, only overall data from the global zone are shown in Fig. 7a while assuming a uniform thickness for AA6056 (i.e., 2 mm). At a nearly comparable total strain, the modified joint specimens did show an increase in strength, particularly in ultimate tensile strength by about 10 %, and reached a level of about 65 % of AA6056-T6. These are average values of three specimens tested for a given joint. Although the global zone tensile behaviour from specimen to specimen for a given joint was comparable within a certain allowance (± 5 MPa in stress and ± 1 % in strain), for statistical analysis more tests are required.

Whereas the strength level for a given joint in the global zone should be governed mainly by the extent of hardening (through GP zones: Fig. 4b), the extent of local deformation determines the location of the fracture site. From the optical image analysis, deformation was found to build-up at about 7 mm from the interface on the Al-side, and is visible as red coloration in Figs. 7b-c. This was the hardness dip, which, being the weakest site in both joints (Fig. 4a), became liable for deformation and strain concentration, and led to fracture at the same location, Figs. 7d-e. The zone “Al-side” alone (data not shown here) exhibited high strain in both cases (≈ 15 %), but was reduced substantially due to the constraint in the global zone (4 %; Fig. 7a). The interface itself had a higher strength [3] and did not undergo deformation in the tensile test (visible as blue coloration in Figs. 7b-c).

It must be recalled with reference to Fig. 7 that features such as cracks in the reaction zone, a pullout or an interfacial fracture as reported recently for dissimilar joints with

aluminium [14,15,33] were not observed. Insofar the interface was sound and mechanically stable. Furthermore, debonding was also not observed under constrained crack tip loading in C(T) specimens. Fracture toughness in terms of CTOD δ_5 is shown in Fig. 8. For a given variant 5 specimens each were tested. That there is some scatter is very common and can be associated with crack deviation. In both cases, fracture toughness of the interface was nearly comparable. Weld interface is reported to decrease fracture toughness due to strength mismatch or weld defects or both [19]. In the present case, fracture toughness has not been degraded and was as good as that of AA6056-T6.

3.4 Fatigue crack propagation

In contrast to monotonic loading, the plastic zone size in cyclic loading is much smaller and interactions with local defects or irregularities in microstructure can become effective and affect the propagation, say by change in the fracture type such as from transcrystalline to intercrystalline fracture due to segregation. Thus, fatigue crack propagation is a very critical test to assess the weld quality. The present data are shown in Fig. 9 in terms of $a-N$ (instead of $da/dN-\Delta K$). The ΔK concept assumes homogeneous material properties. This condition may not necessarily be applicable to welded joints, particularly in the present case when the interface investigated is very thin (Fig. 6). Therefore, to exclude discussions on the applicability of the ΔK concept, the crack length is used as a correlating parameter and should be valid for the comparison since all testing conditions, including load levels, were comparable. The base material data obtained under the same conditions are shown for reference. To exclude artefacts (as the critical state ΔK_c is approached) data only up to 24 mm were considered, although propagation continued further.

Whereas a crack orientation effect in AA6056-T6 was found to be absent, Ti6Al4V exhibited shorter life in L-T than in T-L orientation and is to be attributed to the anisotropic deformation in close packed hexagonal crystal structure. Crack orientation in the welded

specimen was L-T in Ti6Al4V and T-L in AA6056-T6. Therefore, the data in the T-L orientation for Ti6Al4V, although shown for completeness, are *not* considered for comparison. Multiple specimens (totally up to ten and more) were tested for each joint. To retain readability, the data from different specimens of a batch are shown as a shaded range, described by the lower bound and the upper bound specimen. The unmodified joint did already exhibit at least comparable resistance to fatigue crack propagation as the base materials. As mentioned, its ranking was, however, the lowest [4]. Through the joint modification in Fig. 2d the resistance was improved at least by a factor of two (Fig. 9a). Note that, in fact, the interface and defects in dissimilar welds are likely to degrade the fatigue behaviour [16-19]. Insofar, the present results are indeed a success.

Typical crack morphologies in the modified joint specimens are shown in Figs. 9b,c. Usually, the crack at the interface remained confined to the plane of the interface (Fig. 9b). In the unmodified joint specimens, the appearance of the surface crack was similar to that in Fig. 9b, with the difference that traces of deformation were absent and crack separation was insignificant, which is typical for a faster propagation. In some modified joint specimens the crack deviated *away* from the interface into the Al-side as in Fig. 9c, and indicates that the interface had better properties than the surrounding. Given a consideration to problems associated with obtaining a sound interface in a dissimilar weld (e.g. [5,19,29-31,33]), the present results are an achievement, since means such as controlling dispersoids and degree of recrystallisation as in production [56] are not available while welding.

The mid-regime (Paris regime) of AA6056-T6 is found to exhibit low scatter ($\pm 35\%$) and is also insensitive to a number of parameters [57]. Residual stresses on the Al-side should be tensile [3] and thus also not favourable for resistance against fatigue crack propagation. Insofar, the *extent* of improvement at least by a factor of two in the propagation life achieved (Fig. 9a) was surprising. Therefore, extensive fractographic investigations were undertaken

for its clarification. The very common crack propagation feature was striations on the Al-particles adhering to the interface as well as on aluminium in the fusion zone. Basically, crack propagation rate increased (i.e., striations tended to be broader), when Al-particles were large and fracture type in the fusion zone changed from transcrystalline to intercrystalline (due to grain boundary segregation) or became mixed. Here typical fractographic differences of the lower bound specimens in Fig. 9a shown by open circles (unmodified joint) and inverted open triangles (modified joint) are presented.

Corresponding to the modification (Figs. 2c,d), the most evident differences were the decrease of the interface width and the increase in the surrounding Al-portion in the fusion zone, Figs. 10a,d. Whereas fracture in the fusion zone of the unmodified joint specimen was mixed, (Figs. 10a,b), fully transcrystalline fracture with striations was observed in the modified joint specimen (Figs. 10d,e). The faster cooling rate in the latter seems to have increased the solidification rate and decreased the grain boundary segregation, which otherwise provides a preferential fracture path and leads to the intercrystalline fracture as in the unmodified joint specimen. The interface in both cases was covered entirely with small spots which were adhering Al-particles and when protruded, appeared shiny due to higher electron excitation. Otherwise, the background (Ti6Al4V) appeared dull when particle size was small. The Al-particles exhibited striations, were coarse and numerous, and easy to detect on the unmodified joint interface, Fig. 10c. On the modified joint interface such particles were smaller and very finely distributed indicating good binding, and required higher magnification to resolve. Note that striations are visible in Fig. 10c, but not in Fig. 10f. Thus, the factors contributing to the longer life with the interfacial joint modification (Fig. 9a) are the refined fusion zone (Fig. 5) which was under-aged (Fig. 4), the thinner reaction zone (Fig. 6) with good binding and the absence of intercrystalline fracture (Fig. 10e). Here the chamfer

becomes also an important contributor. Fortunately, this surface was defect-free and its fracture was comparable to that of the interface (Figs. 10d,f).

The trend described above continued with further propagation, with the difference that some facetting in the fusion zone and particle pullout occurred in the unmodified joint specimen. In the modified joint specimen striations now tended to become wider, but were still finer, also in the fusion zone. Thereafter (20 mm), the fracture mode started to alter in the unmodified joint specimen. This stage corresponds to rapid crack propagation as ΔK approaches $\Delta K_c (\rightarrow K_{Ic})$. The relationship tacitly meant here is that an increase in the crack length is equivalent to an increase in the ΔK level. Also, it goes without saying that deformation or fracture is dependent on the ΔK level (and not on crack length "a").

Towards the final stage ($a \geq 20$ mm) mixed mode fracture became evident and consisted of striations (fatigue mode) and dimples (ductile tear mode) in the fusion zone of the unmodified joint specimen as shown in Figs. 11a,b. The interface itself in both cases remained unaffected in the sense of fracture features described above. Surprisingly, in the fusion zone of the modified joint specimen only striations were still observed, Figs. 11c,d, and dimples appeared far later ($a > 30$ mm; not shown here). Thus, not only the tensile strength (Fig. 7), but also the $\Delta K_c (\rightarrow K_{Ic})$ value might have been improved through the joint modification.

3.5 Concluding remarks

As already mentioned (in Introduction), the statistical validation is open at present. Nonetheless, the results show that the chamfer did induce improvements in hardness (Fig. 4), microstructure (Figs. 5-6) and strength (Fig. 7). A crack introduces triaxiality in the stress state and insofar fracture toughness and fatigue crack propagation facilitate assessment of stability against defects. Whereas fracture toughness remained unaffected (Fig. 8), fatigue

crack propagation was improved by at least a factor of two (Fig. 9a). Usually, scatter in fatigue crack propagation may vary up to a factor 3 [58]. However, the improvement is more than the scatter level found in AA6056-T6 [57] or the specimen-to-specimen difference (shading in Fig. 9a). Thus, this extent along with the change in the crack path (Fig. 9c) and the differences in the fracture type (Figs. 10-11) clearly show that the improvement brought about by the interfacial modification is a genuine effect.

The overall volume increase in aluminium and the simultaneous reduction of interface are the evident factors (Fig. 2). However, the improvement is not *per se* brought about by the chamfer alone. A number of chain effects need to be pointed out. Among these are the reduced interfacial area and the decreased width of TiAl₃ (Fig. 6), the good binding indicated by finely and uniformly distributed Al-particles (Figs. 10c,f) and the refined fusion zone in the context of grain size (Fig. 5).

The morphological development during solidification is determined by the temperature gradient and the growth rate such that, for example, with the increase in the constitutional supercooling the morphology changes from planar to equiaxed [59]. It seems likely in our case that the increase in volume of the Al-side (good thermal conductivity) coupled with reduced volume of the Ti-side has contributed to an increase in the rate of cooling. In turn, hardness (Fig. 4) and strength (Fig. 7) have been improved through the retained solute that coalesces to GP zones on natural ageing. Moreover, the absence of intercrystalline fracture and the suppression of ductile tearing have contributed to the longer fatigue crack propagation life (Figs. 9-11). Producing good quality welds had always been a challenge. As found here, an increase in the cooling rate in the fusion zone could indeed be a proper measure to refine microstructure and to improve properties, not only for dissimilar, but also for similar welds of precipitation hardenable Al-alloys.

4 Conclusions

Dissimilar butt-welds of Ti6Al4V and AA6056-T6 were produced by laser beam welding. The initial configuration of a straight interface was modified by chamfering Ti6Al4V. Thus, the length of the Al/Ti-interface and the extent of the brittle intermetallic phase $TiAl_3$ were reduced. This configuration has led to the following conclusions:

- 1) The grain size in the fusion zone was reduced and the intermetallic phase formed at the interface was thinner. Specimens could be mechanically tested without formation of cracks in the reaction zone and premature pullout or debonding. In this sense, the welded coupons were sound in both configurations.
- 2) Hardness and tensile strength were slightly higher in the modified joint, whereby the fracture occurred in the hardness dip on the side of AA6056-T6 and the interface remained intact in both cases. Whereas fracture toughness remained nearly comparable in both cases, the resistance to fatigue crack propagation was improved through the joint modification substantially, at least by a factor of two. Here further data are required for statistical validation.
- 3) During fatigue crack propagation partly intercrystalline fracture occurred in the fusion zone of the unmodified joint specimens. This was absent in the modified joint specimens, and completely transcrystalline fracture and striations were observed, not only for the interface adhering Al-particles, but also in the fusion zone. Moreover, ductile tearing occurred after a longer crack length. Such fractographic differences clearly show that the improvement brought about by the joint modification is a genuine effect.
- 4) In addition to the decrease in the interfacial area, the modified configuration is inferred to have induced a faster cooling rate. This has most likely decreased the reaction zone, improved the interfacial binding, reduced the grain size in the fusion zone, avoided grain boundary segregation and retained solute for hardening. In turn, this microstructural refinement has contributed to improved properties.

Acknowledgements

This work was funded by AIRBUS and additionally by GKSS Research Centre. We gratefully acknowledge this financial support. Dr. M. Koçak is now with the GEDIK Holding, Istanbul, Turkey, and Dr. R. Kocik with EADS Space Transportation, Bremen, Germany.

References

1. Kocik R, Kaschel S, Kreimeyer M, Schumacher J, Vollertsen F (2004) In: ICALEO 2004, Proceedings 23rd international conference on application of lasers and electro-optics 2004, San Francisco, California, USA, 4-7 October 2004, Laser Institute of America (LIA), Orlando, Florida, USA, CD-ROM 597
2. Kocik R, Vugrin T, Seefeld T (2006) In: Vollertsen F, Seefeld T (eds) 5. Laser-Anwendungforum, 13-14 September, 2006, Bremen, Laserstrahlfügen: Prozesse, Systeme, Anwendungen, Trends, Strahltechnik, Band 28, BIAS-Verlag, Bremen, Germany, p. 15 (in German)
3. Vaidya WV, Horstmann M, Ventzke V, Petrovski B, Koçak M, Kocik R, Tempus G (2009) Mater Sci Engng Technol (Mat-wiss u Werkstofftech) 40:623
4. Vaidya WV, Horstmann M, Ventzke V, Petrovski B, Koçak M, Kocik R, Tempus G (2009) Mater Sci Engng Technol (Mat-wiss u Werkstofftech) 40:769
5. Bailey N (1986) In: Bailey N (ed) Welding dissimilar metals, The Welding Institute, Cambridge, Great Britain, p. 1
6. Lee C-Y, Lee W-B, Kim J-W, Choi D-H, Yeon Y-M, Jung S-B (2008) J Mater Sci 43:3296
7. Naffakh H, Shamanian M, Ashrafizadeh F (2008) J Mater Sci 43:5300
8. Chen T (2009) J Mater Sci 44:2573
9. Song JL, Lin SB, Yang CL, Ma GC, Liu H (2009) Mater Sci Engng A 509:31
10. Qiu R, Shi H, Zhang K, Tu Y, Iwamoto C, Satonaka S (2010) Mater Charact 61:684
11. Sahin M (2009) Int J Adv Manuf Technol 41:487
12. Lee W-B, Schmuecker M, Mercardo UA, Biallas G, Jung S-B (2006) Scr Mater 55:355
13. Kostka A, Coelho RS, dos Santos J, Pyzalla AR (2009) Scr Mater 60:953
14. Qui R, Iwamoto C, Satonaka S (2009) Mater Sci Technol 25:1189
15. Chen Y, Chen S, Li L (2010) Mater Design 31:227
16. Uzun H, Dalle Donne C, Argagnotto A, Ghidini T, Gambaro C (2005) Mater Design 26:41

17. Tuppen SJ, Bache MR, Voice WE (2005) Int J Fatigue 27:651
18. Lee DG, Jang KC, Kuk JM, Kim IS (2004) J Mater Process Technol 155-156:1402
19. Jiang F, Deng ZL, Sun J, Wei JF (2004) J Mater Engng Perform 13:93
20. Takemoto T, Okamoto I (1988) J Mater Sci 23:1301
21. Fuji A, Kimura M, North TH, Ameyama K, Aki M (1997) Mater Sci Technol 13:673
22. Fuji A, Ameyama K, Kokawa H, Satoh Y, North TH (2001) Sci Technol Weld Joining 6:23
23. Cam G, Koçak M, Dobi D, Heikinheimo L, Siren M (1997) Sci Technol Weld Joining 2:95.
24. Jiangwei R, Yajiang L, Tao F (2002) Mater Lett 56:647
25. Ege ES, Inal OT (2000) J Mater Sci Lett 19:1533
26. Dressler U, Biallas G, Mercado UA (2009) Mater Sci Engng A 526:113
27. Sun Z, Ion JC (1995) J Mater Sci 30:4205
28. Imaizumi S (1996) Weld Int 10: 593
29. Skoda P, Dupak J, Michalicka P (1996) In: Proceedings international welding conference, Japan Slovak welding symposium, Tatranske Matliare, Tatranska Lomnica, paper 30, p. 157
30. Majumdar B, Galun R, Weisheit A, Mordike BL (1997) J Mater Sci 32:6191
31. Cabibbo M, Marrone S, Quadrini E (2005) Weld Int 19:125
32. Chen Y, Chen S, Li L (2009) Int J Adv Manuf Technol 44:265
33. Jácome LA, Weber S, Leitner A, Arenholz E, Bruckner J, Hackl H, Pyzalla AR (2009) Adv Engng Mater 11:350
34. Bruckner J, Wagner J, Arenholz E (2005) In: Kaufmann H (ed) Proceedings 2nd international light metals technology conference 2005, 8-10 June 2005, St. Wolfgang, Austria, p. 275
35. Parker SP (ed) (1989) McGraw-Hill dictionary of scientific and technical Terms, 4th edn. McGraw-Hill Book Company, New York, USA, p. 2056
36. Ibid. p. 252
37. Dif R, Bes B, Ehrström JC, Sigli C, Warner TJ, Lassince P, Ribes H (2000) Mater Sci Forum 331-337:1613
38. Dif R, Warner T, Bes B, Lequeu P, Ribes H, Lassince P (2001) In: Tiryakioglu M (ed) Advances in the metallurgy of aluminium alloys, ASM International, Materials Park, USA, p. 390
39. NN, ARAMIS, Optical Deformation Analysis System; (www.gom.com)

40. NN (2005) Annual book of ASTM standards, section three, volume 03.01, ASTM International, West Conshohocken, PA, USA, p. 628
41. Ibid. p. 557
42. Schwalbe K-H, Heerens J, Zerbst U, Pisarski H, Koçak M (2002) EFAM GTP 02-the GKSS test procedure for determining the fracture behaviour of materials, GKSS Report 2002/24
43. Schwalbe K-H (1995) ASTM STP 1256:763
44. Mazur M (1992) Weld Int 6:929
45. Kou S (2003) Welding metallurgy, 2nd edn. John Wiley & Sons, Hoboken, New Jersey, USA, pp. 359-371
46. Cao X, Rivaux B, Jahazi M, Cuddy J, Birur A (2009) J Mater Sci 44:4557
47. Tanaka M, Warner T (2003) Revue de Métallurgie 100:463
48. Fabregue D, Deschamps A, Suery M (2005) Mater Sci Technol 21:1329
49. Staron P, Vaidya WV, Koçak M (2009) Mater Sci Engng A 525:192
50. Jain A, Basu B, Manoj Kumar BV, Harshavardhan, Sarkar J (2010) Acta Mater 58:2313
51. Iqbal N, van Dijk NH, Offerman SE, Geerlofs N, Moret MP, Katgerman L, Kearley GJ (2006) Mater Sci Engng A 416:18
52. Wang Q, Li YX, Li XC (2003) Metall Mater Trans A 34A:1175
53. Faraji M, Wright JP, Katgerman L (2010) Mater Lett, doi:10.1016/j.matlet.2010.01.028
54. Okamoto H (1993) J Phase Equilibria 14:120
55. Sujata M, Bhargava S, Sangal S (1997) J Mater Sci Lett 16:1175
56. Warner T, Dif R, Ehrström JC, Lassince P (2000) In: New metallic materials for the structure of aging aircraft, RTO AVT Workshop, 19-20 April 1997, Corfu, Greece, NATO RTO MP-25 meeting proceedings, April 2000, Neuilly-sur-Seine, France, p. 10-1.
57. Vaidya WV, Horstmann M, Angamuthu K, Koçak M (2010) MP Mater Testing 52:300
58. Clark WG Jr, Hudak SJ Jr (1975) J Test Eval 3:454
59. Kou S (2003) Welding metallurgy, 2nd edn. John Wiley & Sons, Hoboken, New Jersey, USA, pp. 145-215

Figure captions

Fig. 1 The passenger seat track as a laser beam welded dissimilar joint, (conceptual design after AIRBUS. The total height of the assembly is about 61 mm, the web height about 45 mm and the aluminium alloy flange width about 50 mm; drawing not to scale).

Fig. 2 Butt-weld configuration of the dissimilar joint AA6056-T6 and Ti6Al4V produced by split-beam laser welding. Essential features of the welding process are shown schematically in a) and b). Since only the Al-alloy was melted, regions starting from the weld interface on the Al-side are shown in c) and d). Initially, straight Ti6Al4V sheet was used, c), and was modified later by the chamfer, d). The vertical line shows the notch location in the cross section for fatigue crack propagation and fracture toughness testing, (see Fig. 3 for the dimensions of the U-slot and the specimen orientations).

Fig. 3 Dimensions of the machined U-slot used for the intake of Ti6Al4V sheet, a), and a typical laser beam welded coupon along with different specimens extracted, b). Locations of the fusion zone and the weld interface are also marked, (dimensions in mm).

Fig. 4 The hardness variation, a) and b), and its correlation to hardening constituents, c), in the unmodified and the modified joint specimens on the AA6056-T6 side. The approximate location of the hardness traverse and the respective symbols are shown in the insets in a) and hardness values in the shaded frame are displayed on a magnified scale in b). Abbreviations used are as follows; BM: base material, HAZ: heat affected zone, FZ: fusion zone, LBW: laser beam welding, SS: solid solution, and heat treatments (temper designations) T4: under-aged and T6: peak-aged. The grey horizontal bands in c) indicate the microhardness level reached after a given heat treatment, (Fig. 4c is based on the literature, see [3]).

Fig. 5 A schematic representation of the interfacial plane, a), and how it was reached for metallography, b). The microstructural differences in the interfacial plane, as imaged in the

back scattered electron mode (material contrast) in SEM, are shown in c) and d) for the unmodified and the modified joint specimens. Variations in grain orientation are visible as the difference in gray colour, (specimens unetched).

Fig. 6 Difference in the morphology of the intermetallic phase in the reaction zone imaged with back scattered electrons; unmodified joint, a) and modified joint, b).

Fig. 7 Improved tensile strength in the global zone after the joint modification. Gauge length divisions are shown in the inset and consists of the central mixed zone (10 mm: 5 mm each on either side of the from the interface), two additional zones on the Ti-side and the Al-side (5 mm each) for local properties and the global zone (20 mm) compromising all these zones. The data along with the tensile curves in the global zone are shown in a), optical images of the deformation pattern at 200 MPa in b) and c), and the fracture location in d) and e).

Fig. 8 Resistance to fracture in terms of crack tip opening displacement, CTOD δ_5 . The horizontal bands show the base material data for Ti6Al4V and AA6056-T6.

Fig. 9 Improved resistance to fatigue crack propagation through the joint modification. The base material data in L-T and T-L orientations are shown for reference in a) and the crack path in the modified joint in b) and c). Note the crack path deviation *away* from the interface and into the Al-side in c).

Fig. 10 Fractographic differences after stabilization of fatigue crack propagation in the unmodified, a)-c), and the modified joint specimens, d)-f). The frames on the overall view mark approximately the respective area enlarged. Note the finer striations and the absence of intercrystalline fracture mode in the modified joint specimen.

Fig. 11 Fracture mode variation in very rapid fatigue crack propagation region at and after 25 mm in unmodified joint specimen, a)-b), and modified joint specimen, c)-d). The frames in

a) and c) mark approximately the area enlarged in b) and d). Note the persistence of striations and the absence of dimples in the modified joint specimen.

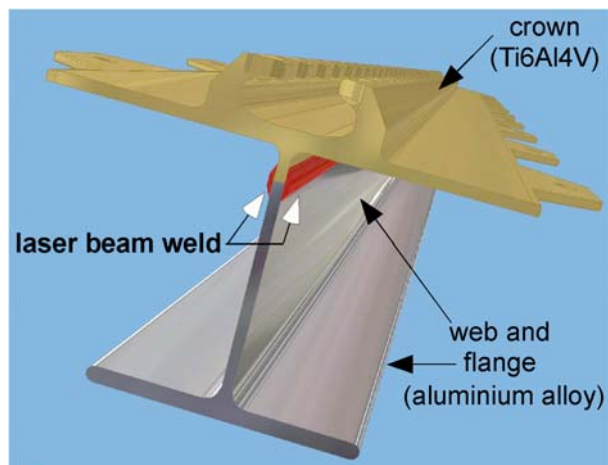


Fig. 1 The passenger seat track as a laser beam welded dissimilar joint, (conceptual design after AIRBUS. The total height of the assembly is about 61 mm, the web height about 45 mm and the aluminium alloy flange width about 50 mm; drawing not to scale).

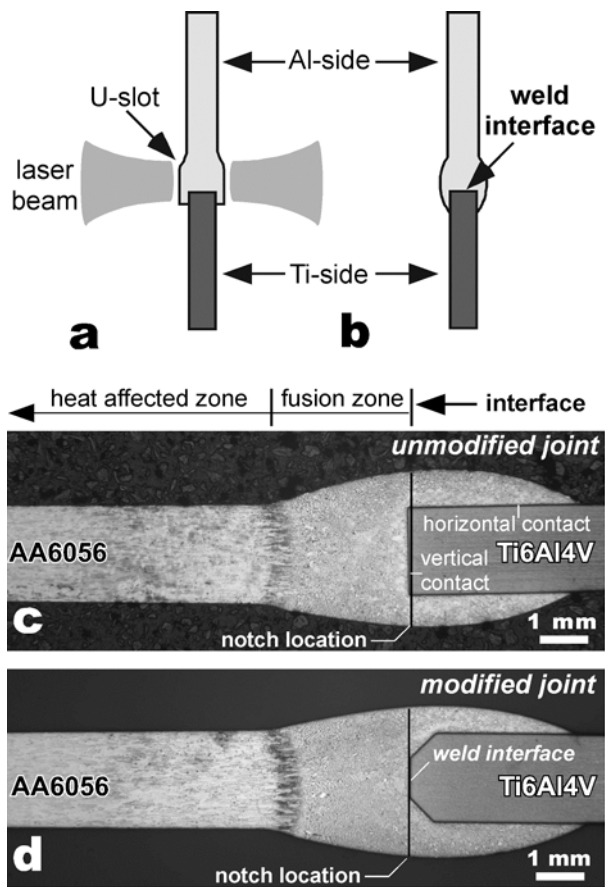


Fig. 2 Butt-weld configuration of the dissimilar joint AA6056-T6 and Ti6Al4V produced by split-beam laser welding. Essential features of the welding process are shown schematically in a) and b). Since only the Al-alloy was melted, regions starting from the weld interface on the Al-side are shown in c) and d). Initially, straight Ti6Al4V sheet was used, c), and was modified later by the chamfer, d). The vertical line shows the notch location in the cross section for fatigue crack propagation and fracture toughness testing, (see Fig. 3 for the dimensions of the U-slot and the specimen orientations).

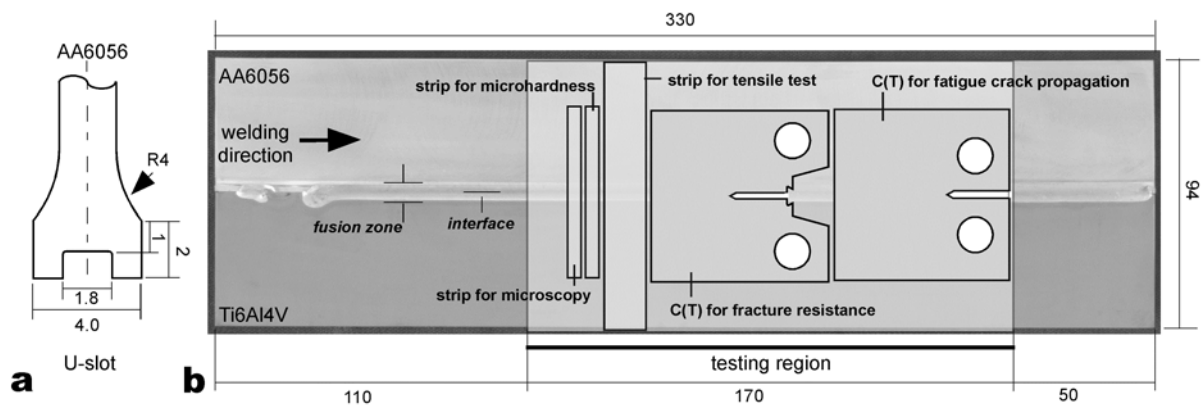


Fig. 3 Dimensions of the machined U-slot used for the intake of Ti6Al4V sheet, a), and a typical laser beam welded coupon along with different specimens extracted, b). Locations of the fusion zone and the weld interface are also marked, (dimensions in mm).

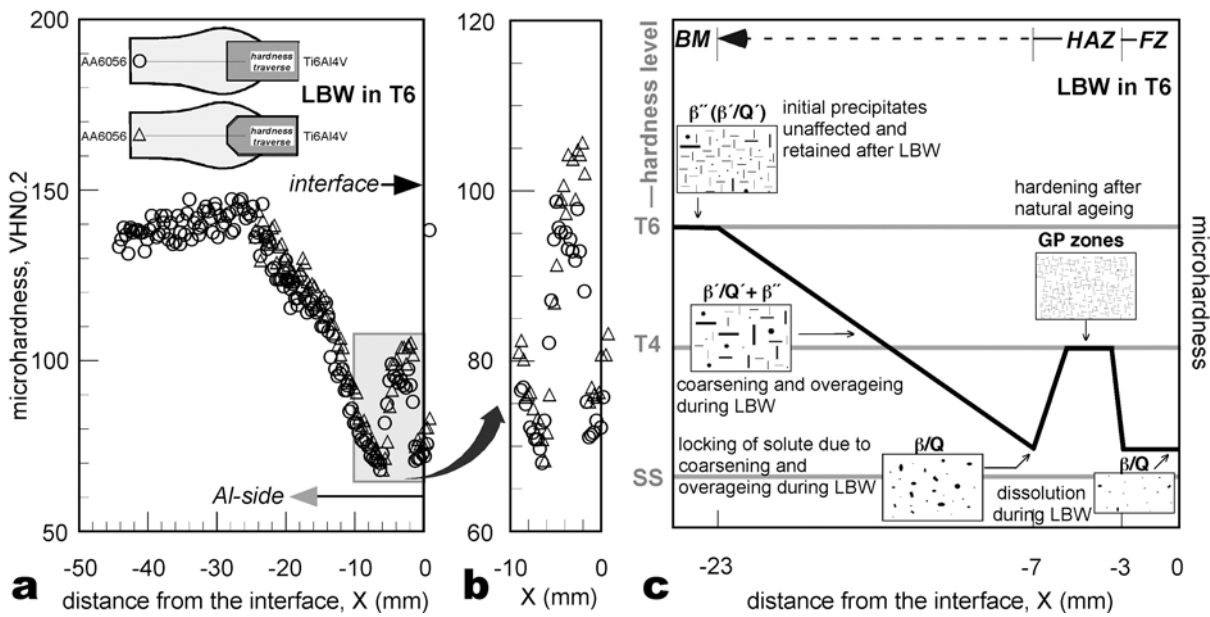


Fig. 4 The hardness variation, a) and b), and its correlation to hardening constituents, c), in the unmodified and the modified joint specimens on the AA6056-T6 side. The approximate location of the hardness traverse and the respective symbols are shown in the insets in a) and hardness values in the shaded frame are displayed on a magnified scale in b). Abbreviations used are as follows; BM: base material, HAZ: heat affected zone, FZ: fusion zone, LBW: laser beam welding, SS: solid solution, and heat treatments (temper designations) T4: under-aged and T6: peak-aged. The grey horizontal bands in c) indicate the microhardness level reached after a given heat treatment, (Fig. 4c is based on the literature, see [3]).

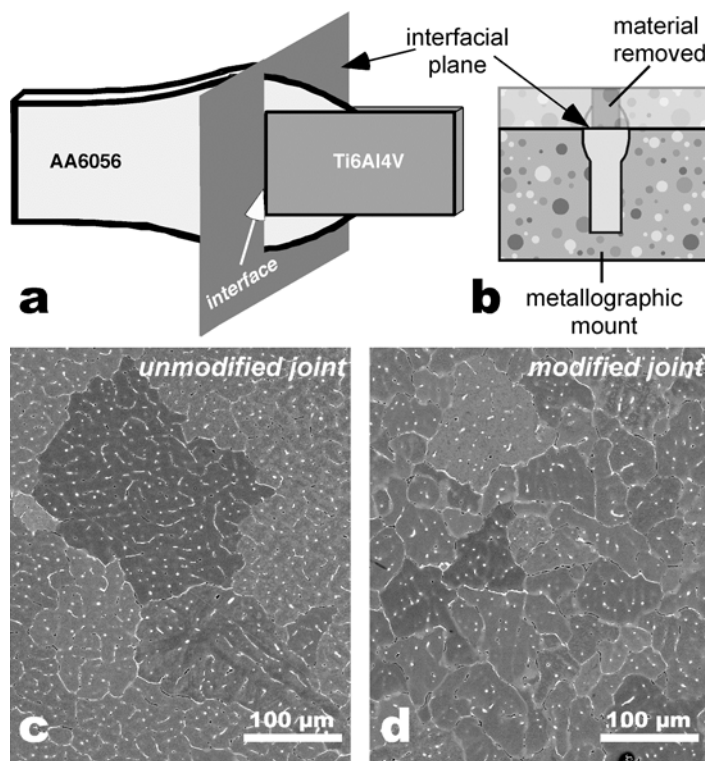


Fig. 5 A schematic representation of the interfacial plane, a), and how it was reached for metallography, b). The microstructural differences in the interfacial plane, as imaged in the back scattered electron mode (material contrast) in SEM, are shown in c) and d) for the unmodified and the modified joint specimens. Variations in grain orientation are visible as the difference in gray colour, (specimens unetched).

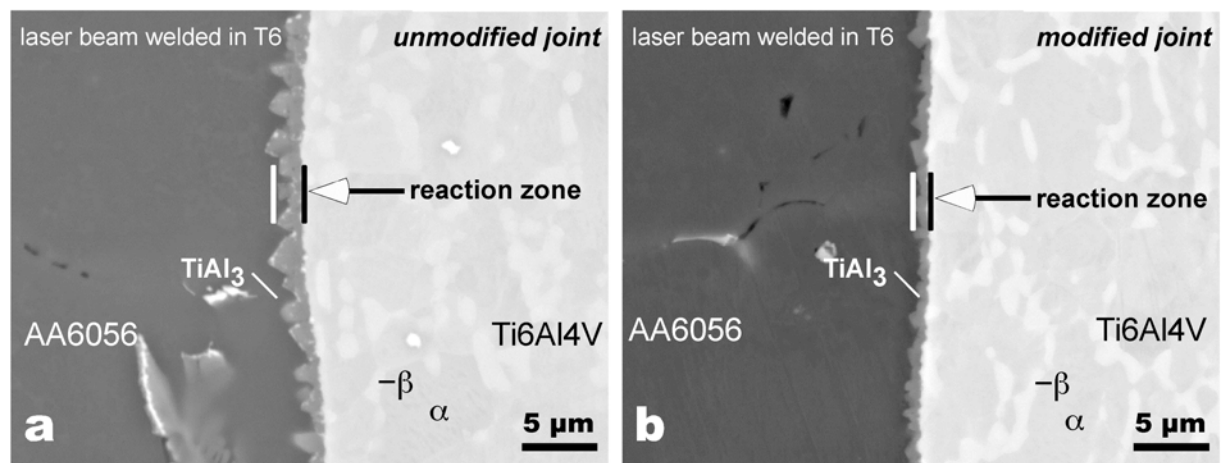


Fig. 6 Difference in the morphology of the intermetallic phase in the reaction zone imaged with back scattered electrons; unmodified joint, a) and modified joint, b).

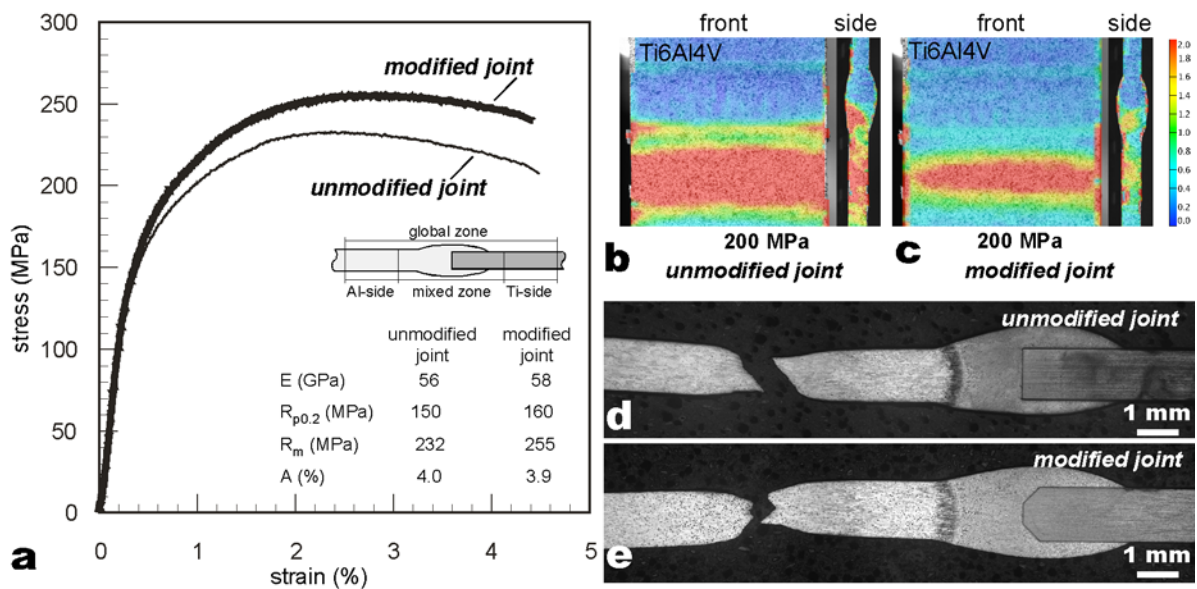


Fig. 7 Improved tensile strength in the global zone after the joint modification. Gauge length divisions are shown in the inset and consists of the central mixed zone (10 mm: 5 mm each on either side of the from the interface), two additional zones on the Ti-side and the Al-side (5 mm each) for local properties and the global zone (20 mm) compromising all these zones. The data along with the tensile curves in the global zone are shown in a), optical images of the deformation pattern at 200 MPa in b) and c), and the fracture location in d) and e).

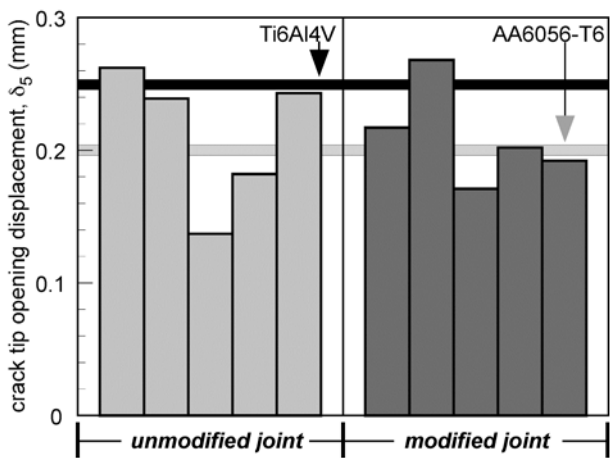


Fig. 8 Resistance to fracture in terms of crack tip opening displacement, CTOD δ_5 . The horizontal bands show the base material data for Ti6Al4V and AA6056-T6.

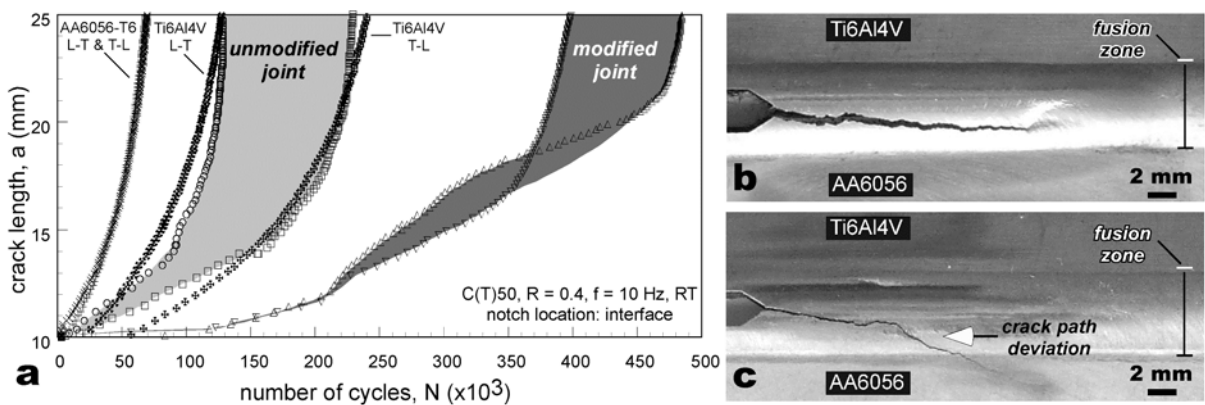


Fig. 9 Improved resistance to fatigue crack propagation through the joint modification. The base material data in L-T and T-L orientations are shown for reference in a) and the crack path in the modified joint in b) and c). Note the crack path deviation *away* from the interface and into the Al-side in c).

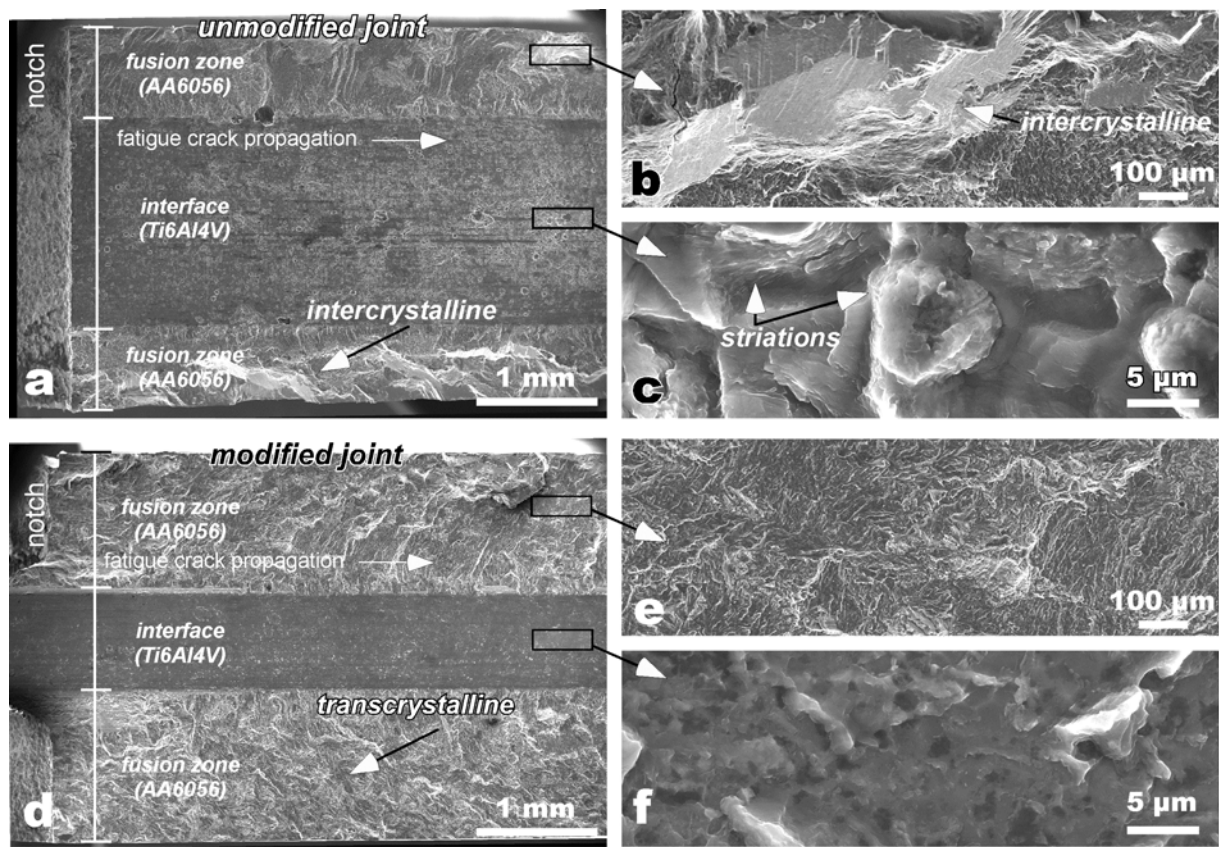


Fig. 10 Fractographic differences after stabilization of fatigue crack propagation in the unmodified, a)-c), and the modified joint specimens, d)-f). The frames on the overall view mark approximately the respective area enlarged. Note the finer striations and the absence of intercrysalline fracture mode in the modified joint specimen.

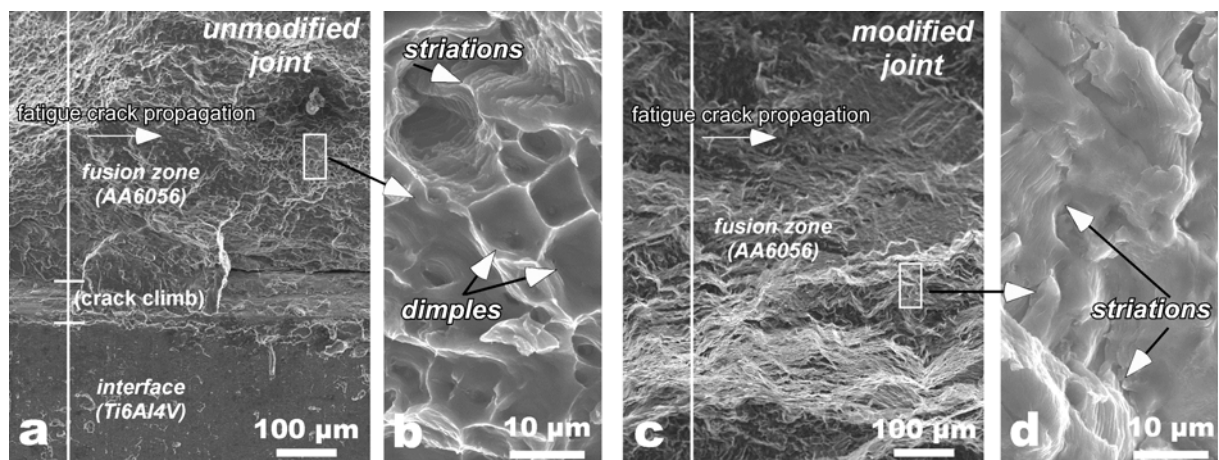


Fig. 11 Fracture mode variation in very rapid fatigue crack propagation region at and after 25 mm in unmodified joint specimen, a)-b), and modified joint specimen, c)-d). The frames in a) and c) mark approximately the area enlarged in b) and d). Note the persistence of striations and the absence of dimples in the modified joint specimen.

Table 1 Chemical composition of the precipitation hardenable alloy AA6056 and Ti6Al4V investigated (in wt %)

Alloy	Elements (wt %)											
	Si	Mg	Cu	Mn	Cr	Fe	Zn	C	N ₂	Al	V	Ti
AA6056	0.93	0.75	0.79	0.618	0.016	0.158	0.169	-	-	Balance	-	-
Ti6Al4V	-	-	-	-	-	0.17	-	0.014	0.012	6.2	4.7	Balance

Table 2 Parameters used for dissimilar butt-welding AA6056-T6 and Ti6Al4V with Nd:YAG laser (type Trumpf HL4006D)

Parameter	Value
Laser power utilized	3.5 kW in continuous wave mode
Beam split ratio	1:1 (i.e., 2 x 1.75 kW)
Focal length	200 mm
Beam diameter on the work piece	ca. 7 mm
Welding speed	0.22 m/min
Energy input per unit length	955 kJ/m
Shielding gas	Argon 55 l/min

Table 3 Energy dispersive X-ray analysis of the typical particles in the fusion zone

Location	Element											
	Mg		Al		Si		Mn		Fe		Cu	
	Wt %	At %	Wt %	At %	Wt %	At %	Wt %	At %	Wt %	At %	Wt %	At %
Intragranular globular particle	4.98	7.25	42.09	55.20	11.05	13.92	1.47	00.95	2.24	1.42	38.17	21.26
Intragranular lenticular particle	1.35	1.81	55.80	68.87	11.85	13.80	0.30	0.18	0.70	0.41	29.01	14.94
Grain boundary particle	1.87	2.58	60.82	75.36	3.48	4.14	1.09	0.66	0.54	0.33	32.19	16.94
Particle-free matrix	0.98	1.09	98.88	98.78	0.14	0.13	n.d.*	n.d.*	n.d.*	n.d.*	n.d.*	n.d.*

n.d.*: not detected due to very small peak size and background scattering.